Computer Methods and Programs in Biomedicine 226 (2022) 107148

Contents lists available at ScienceDirect

Computer Methods and Programs in Biomedicine

journal homepage: www.elsevier.com/locate/cmpb

Automatic modeling of dynamic drug-hERG channel interactions using three voltage protocols and machine learning techniques: A simulation study

Fernando Escobar, Julio Gomis-Tena, Javier Saiz, Lucía Romero*

Centro de Investigación e Innovación en Bioingeniería, Universitat Politècnica de València

ARTICLE INFO

Article history:
Received 1 February 2022
Revised 12 September 2022
Accepted 19 September 2022

Keywords:
Drug modeling
In-silico model
Ion channels
hERG blocker
I_{Kr} blocker
Machine learning

ABSTRACT

Background: Assessment of drug cardiac safety is critical in the development of new compounds and is commonly addressed by evaluating the half-maximal blocking concentration of the potassium human ether-à-go-go related gene (hERG) channels. However, recent works have evidenced that the modelling of drug-binding dynamics to hERG can help to improve early cardiac safety assessment. Our goal is to develop a methodology to automatically generate Markovian models of the drug-hERG channel interactions.
Methods: The training and the test sets consisted of 20800 and 5200 virtual drugs, respectively, distributed into 104 groups with different affinities and kinetics to the conformational states of the channel. In our system, drugs may bind to any state (individually or simultaneously), with different degrees of preference for a conformational state and the change of the conformational state of the drug bound channels may be restricted or allowed. To model such a wide range of possibilities, 12 Markovian chains are considered. Our approach uses the response of the drugs to our three previously developed voltage clamp protocols, which enhance the differences in the probabilities of occupying a certain conformational state of the channel (open, closed and inactivated). The computing tool is comprised of a classifier and a parameter optimizer and uses linear interpolation, support vector machines and a simplex method for function minimization.
Results: We propose a novel methodology that automatically generates dynamic drug models using Markov model formulations and that elucidates the states where the drug binds and unbinds and the preferential binding state using data obtained from simple voltage clamp protocols that captures the preferential state-dependent binding properties, the relative affinities, trapping and non-trapping dynamics and the onset of I_{Kr} block. Overall, the tool correctly predicted the class of 92.04% of the drugs and the model provided by the tool accurately fitted the response of the target compound, the mean accuracy being 97.53%. Moreover, generation of the dynamic model of an I_{Kr} blocker from its response to our voltage clamp protocols usually takes less than an hour on a common desktop computer.
Conclusion: Our methodology could be very useful to model and simulate dynamic drug–hERG channel interactions. It would contribute to the improvement of the preclinical assessment of the proarrhythmic risk of drugs that inhibit I_{Kr} and the efficacy of antiarrhythmic I_{Kr} blockers.

1. Introduction

The human ether-à-go-go related gene (hERG) is responsible for one of the most important repolarizing currents in the heart, the rapid component of the delayed rectifier current (I_{Kr}). This current highly affects the action potential duration and its blockade is commonly associated with the appearance of a fatal arrythmia known as Torsade de Pointes. Therefore, drugs inhibiting this current are potentially hazardous [1]. For this reason, the evaluation of the in vitro block potency, quantified by the IC_{50} (drug concentration at which the current is half blocked), is the most common test to assess the cardiac safety of new compounds [2]. While this approach has prevented potentially dangerous drugs from reaching the market, it may have stopped the development of safe compounds [3]. Current guidelines acknowledge the use of IC_{50} as a

* Corresponding author at: Centro de Investigación e Innovación en Bioingeniería (Ci2B), Universitat Politècnica de València, Camino de Vera, s/n, 46022 Valencia, Spain.
E-mail address: lromero@ci2b.upv.es (L. Romero).

https://doi.org/10.1016/j.cmpb.2022.107148

safety parameter. However, IC_{50} has been reported to show high degrees of variability depending on the voltage clamp protocol, temperature or cell type used to measure it [4–10]. Some experimental studies showed variations higher than 10-fold when only changing the voltage protocol [11,12].

Previous studies have shown that determining the compound dynamics is crucial to simulate drug effects more accurately [12] and to improve the in silico assessment of proarrhythmia risk [13]. In this study, we combine in silico simulations using electrophysiological models with supervised machine learning techniques to elucidate the preferential state for drug binding and to elaborate dynamic drug models. The models obtained by our approach can be used to study the effects of I_{Kr} blockers cardiac electrophysiology for different purposes, such as cardiac safety and the study of the efficacy of antiarrhythmic drugs. They may have a relevant impact now that new regulatory guidelines have included modeling and simulation of drug-channel interactions as a source of evidence in the development of new compounds [14].

2. Material and methods

2.1. Drug Models

I_{Kr} was simulated using the human ventricular Markov chain model proposed by Fink et al. [15]. It has five states: three closed states, namely, C_3, C_2, C_1, an open state, called O, and an inactivated state, labeled I. Five new states were included to simulate drug-channel interaction and they were named C_{3d}, C_{2d}, C_{1d}, O_d and I_d. All channel configurations are shown in Fig. 1.

Ion channel-drug interaction depends on a series of properties such as preferential binding to certain states and distinct affinities to these states. In order to create the set of virtual compounds for this study, we first gathered information available in the literature obtained from experiments with well characterized I_{Kr} blockers. Most compounds, such as dofetilide or verapamil bind to the open or inactivated state [13,16–18], but there are also some compounds like ketoconazole and BeKm-1 that preferentially block the channel in the closed state [19–21]. Moxifloxacin has shown a rapid open state block and possibly a component of closed state block [22]. In addition, there are drugs that have a tendency to be trapped within the closed state, like dofetilide [23], nifekalant [23], bepridil [23,24], domperidone [24], E-4031 [24] and terfenadine [18,24]. Other drugs, like amiodarone, droperidol, haloperidol [24] do not exhibit that tendency. Some experiments suggest that cisapride has a tendency to be trapped in the closed state [25], although there is evidence of the opposite as well [18,24]. Taking the abovementioned aspects into account, we chose to simulate not only open and inactivated state blocking, but also closed state blocking and trapping and non-trapping dynamics, as suggested by the experimental studies already mentioned. Moreover, the study performed by Perrin and coworkers [26] stated that cisapride, dofetilide, terfenadine, and astemizole and dl-sotalol bind to the open and inactive state and obtained a ratio between state affinities ranging from 4 to 70-fold. They did not find state dependent preference for the open or inactivated state in erythromycin, perhexiline, and quinidine. In our study, we chose to extend the ratio between preferential and non-preferential state affinities from 3 to 100-fold and we also considered compounds without state preference.

Taking into account the abovementioned aspects, we simulated a series of drugs with a wide variety of affinities and kinetics. We considered drugs which bind exclusively to the open (Fig. 1-A, B), inactivated state (Fig. 1-C, D) or closed (Fig. 1-E, F), drugs interacting simultaneously with both the open and inactivated states (Fig. 1-G, H) or the closed and open states (Fig. 1-I, J), and finally, drugs which bind simultaneously to all states (Fig. 1-K, L). Moreover, we considered both possibilities, restricting or allowing drug bound channels to change their conformational state unless unbinding occurs (Fig. 1-A, C, E, G, I, K and Fig. 1- B, D, F, H, J, L), and we labeled those compounds stuck and unstuck, respectively. Microscopic reversibility was imposed by equaling the product of the transition rates going clockwise to the anticlockwise product in closed loops. Drug kinetics were thoroughly studied by using a wide range of values for the diffusion (k) and dissociation (r) rates for all the configurations. Diffusion rates were the same for all the states and varied from 10 to 1 $\mu M^{-1}s^{-1}$ and dissociation rates ranged from 10^{-3} to 10^{-1} s^{-1} for the preferential binding state. As the maximum ratio between the preferential and non-preferential dissociation rates is 100, the total range for the dissociation rates is from 10^{-3} to 10 s^{-1}. The range of kinetics was adjusted from our previous paper [12] to avoid the simulation of too fast and too slow onsets of I_{Kr} block. Drugs were labeled according to their preferential binding state and a total of 13 classes were simulated. Open, Inactivated and Closed are compounds interacting only in the open, inactivated and closed states, respectively. OpenI, InactiveO and OI are drugs binding to both the open and inactive states with preference for the open state, inactivated state and with the same preference for both states, respectively. OpenC, ClosedO, and CO represent drugs that bind to the closed and open states simultaneously but with higher affinity to the open state, closed state, or with equal affinity for both states respectively. Finally, OpenCI, InactiveCO, ClosedOI and COI are compounds binding simultaneously to the three states with higher affinity to the open, inactivated or closed states and with the same affinity to all of them, respectively.

A total of 26000 virtual drugs were generated for this study. Eight sets of 2600 virtual drugs (stuck and unstuck variants of 13 classes with 200 drugs per class) were created for training purposes by using random values within the abovementioned ranges for the diffusion and the dissociation rates from the preferential state. Diffusion rates (k) were shared for all sets, and we set the ratio between the dissociation rates from the preferential states over those from the non-preferential states to 100, 30, 10 and 3 and we labeled the drugs 100R, 30R, 10R and 3R, respectively. For example, an InactiveO 100R drug with a dissociation rate of 10^{-1} s^{-1} for the inactive state has a dissociation rate of 10 s^{-1} for the open state. Another eight different sets of 650 compounds (stuck and unstuck variants of 13 classes and 50 drugs per class) were created for testing purposes using another random seed. The drugs were created using Matlab by selecting random values from a uniform distribution created with the abovementioned boundaries. Additionally, dofetilide was simulated using a model previously developed by Romero et al. [27].

2.2. Stimulation Protocols

Our three previously developed [12] voltage clamp protocols, named P40, P0 and P-80, which maximize the probability of the channels to occupy each conformational state, were used (Fig. 2, left column). The protocols consisted of a 5 s variable voltage conditioning step followed by a 0.2 s test pulse at -60 mV repeated at 5.4 s intervals, from a holding potential of -80 mV. The conditioning step is applied at -80, 0 and 40 mV for P-80, P0 and P40, respectively. In the case of P-80, a 0.5 ms prepulse at 20 mV was incorporated and the 0.2 s test pulse was fixed at −50 mV. Temperature was set at 22°C, intracellular potassium concentration was fixed at 130 mM and the extracellular one at 4 mM.

2.3. Parameters

Hill plots were created by measuring the tail current amplitude at the steady state (Fig. 2, second column) and plotting its normalized value as a function of the decimal logarithm of the drug con-

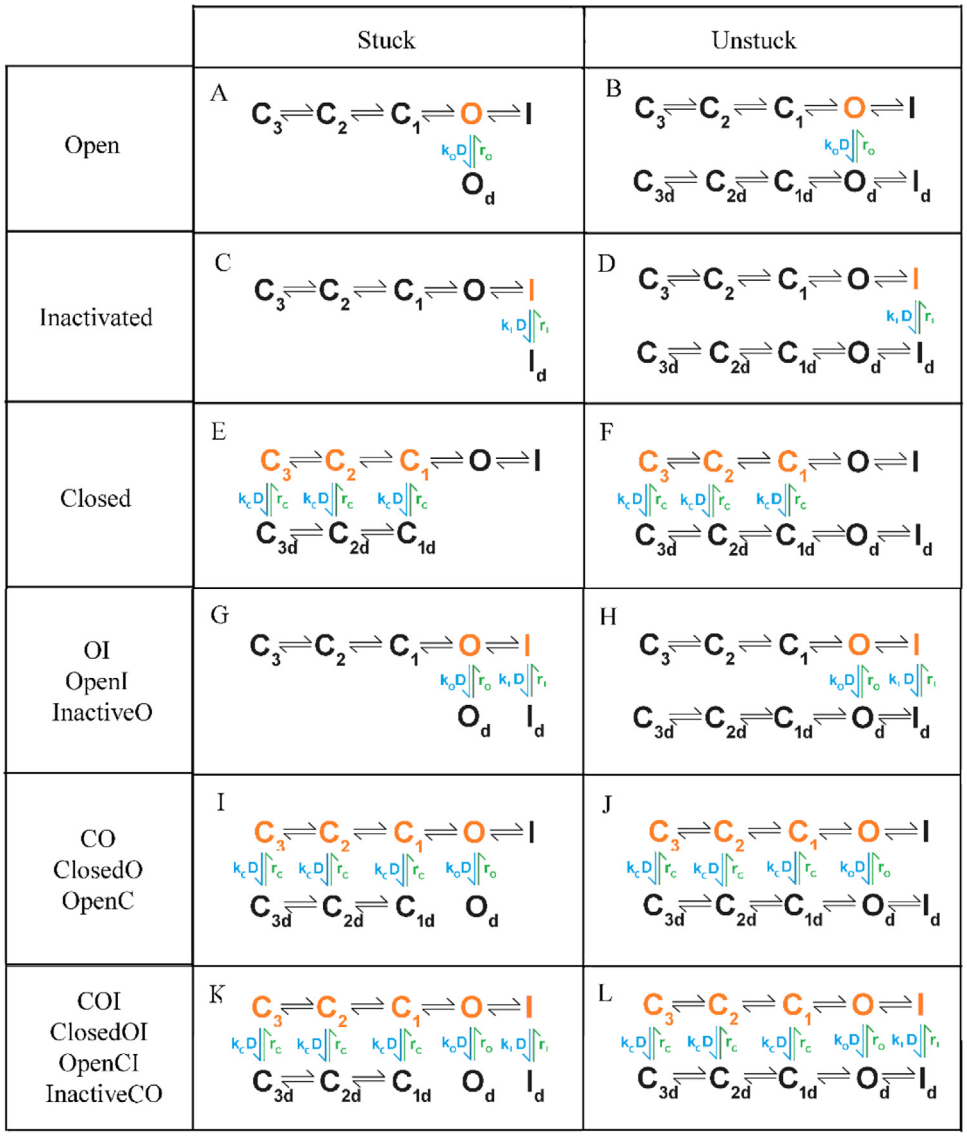

Fig. 1. I_{kr} Markov models showing drug-bound states (C_{3d}, C_{2d}, C_{1d}, O_d and I_d) and drug-free states (C_3, C_2, C_1, O and I). k_c, k_o and k_i are the diffusion rates for the closed, open and inactivated states respectively. r_c, r_o, r_i are the dissociation rates for the closed, open and inactivated states respectively. D is the drug concentration.

centration (Fig. 2, third column), as in previous studies [12]. The number of sweeps of the voltage clamp protocol depends on the specific compound, as the block is measured at the steady state. A total of 2.340.000 simulations were performed. The IC_{50} values obtained with P-80, P0 and P40 were called $IC_{50,P\text{-}80}$, $IC_{50,P0}$, $IC_{50,P40}$, respectively. The onset of I_{Kr} block at the IC_{50} concentration was also analyzed for each protocol (Fig. 2, last column) by plotting the normalized tail I_{Kr} amplitudes for each sweep of the voltage clamp protocol as a function of time and obtaining the time constants with P-80, P0 and P40, which were called $\tau_{P\text{-}80}$, τ_{P0}, τ_{P40}, respectively. The biexponential behavior observed when the compound binds to the channel at 0 mV (Fig. 2, top panel, third column) is consistent with previously observed experimental results [28].

2.4. Unicellular simulations

Action potentials were simulated at 1 Hz using a version of the O'Hara endocardial model [29]. The I_{Kr} formulation was replaced by the Markov model of I_{Kr} from Fink et al. [15], which was scaled to elicit the same peak I_{Kr} value as the original O'Hara model at 1 Hz, as in previous works [12,27].

2.5. Classifier and parameter optimizer

The classification algorithm used Support Vector Machines (SVM) and linear interpolation, which were generated from the parameters calculated from the training compounds using automatic Matlab functions. SVM were generated with IC_{50} data and linear interpolation was applied to the IC_{50}s and time constants datasets. SVM were used to separate certain groups of compounds (as explained in the Results Section and illustrated in Fig. 4) and linear interpolation was used to obtain the distance from the point defined by the parameters of the target compound to the lines corresponding to each of the virtual drug groups.

The optimization algorithm used a Matlab function implementing the iterative Nelder-Mead simplex algorithm [30] with boundary conditions in line with the diffusion and dissociation rates used to generate the training compounds, as in our previous study [27].

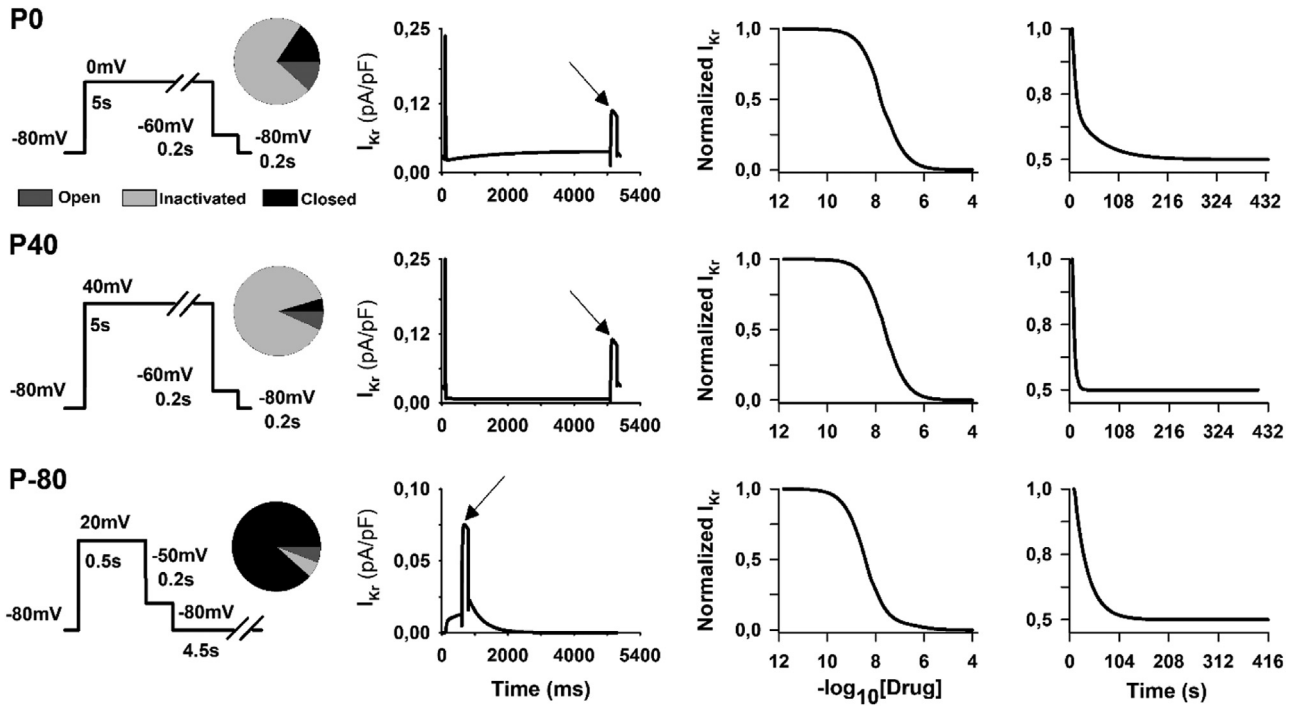

Fig. 2. Effects of the three voltage clamp protocols: P0 (top), P40 (middle) and P-80 (bottom) for a ClosedOI compound. Representation of the voltage protocols and the relatives state occupancies for each of them as an inset of a pie chart (first column), steady state of the time course of the current with each voltage protocol under exposure to the respective IC_{50} concentration during a sweep and arrows indicate the measure point (second column), Hill plots of a virtual drug obtained with the three protocols (third column) and onset of I_{Kr} block (normalized tail current amplitudes for each sweep of the voltage clamp protocol are plotted as a function of time at the corresponding IC_{50} concentration, last column).

3. Results

In order to automatically generate the mathematical dynamic model of a drug-channel interaction, we developed a methodology that first classifies the new compound into the thirteen classes (see the methods section) and then, fits the corresponding binding and unbinding rates. Moreover, we used this methodology to automatically generate a dynamic model of dofetilide, a well-know and high-affinity I_{Kr} blocker. As the six variables ($IC_{50,P-80}$, $IC_{50,P0}$, $IC_{50,P40}$ and τ_{P-80}, τ_{P0}, τ_{P40}.) that are the inputs needed for our system are not available in the literature, we simulated them using a previously developed model that was fitted to reproduce experimental data obtained with other voltage clamp protocols [27]. Fig. 3 shows the simulated Hill plots using the three protocols and the onset of I_{Kr} block at the respective IC_{50} values (solid lines). The results obtained with the new model automatically generated by our novel approach are also superimposed (dashed lines) and they are very similar. The errors obtained by our optimized model were 3.8%, 3.5% and 13% for the current inhibition at the IC_{50} for the P0, P40 and P-80 protocols respectively and 0.23% and 3.7% for the diffusion and dissociation rates, respectively. A very good concordance between the target (inputs to the system) and the results simulated with the model generated automatically by our pipeline is observed.

4. Drug class assignment

Our previously developed voltage clamp protocols were applied to the 26000 training virtual drugs and the Hill-plots were simulated. Fig. 2 illustrate the results obtained with a ClosedOI drug. The parameters were then computed for each virtual drug. Fig. 4 shows an example of 3D scattered plots of the IC_{50} values ($IC_{50,P-80}$, $IC_{50,P0}$, $IC_{50,P40}$) for a subset of the simulated drugs containing the thirteen classes. This figure shows that the IC_{50} values of drugs of the same class obtained with the three protocols show a linear tendency and hyperplanes could be used to distinguish three groups of drugs with closed (top), open (middle) or inactivated (bottom) state preference, except for the drugs with the same affinity to the binding states (OI, COI and CO). This prompted us to design a classifier using support vector machines (SVM) and linear interpolation in order to assign the class to the new compounds. SVM were applied only to the IC_{50} while linear interpolation was used for both variables the top table of Fig. 5 shows the confusion matrix of the developed classifier. The labels on the right are the true classes of the drugs, and the bottom labels are the predicted classes. The main diagonal boxes represent the correctly classified drugs (blue), and the remaining boxes correspond to misclassified drugs (orange). The number of drugs corresponding to each box of the matrix is included. The two rightmost columns show the true positive and the negative rates in percentage and the two bottommost rows show the positive and the negative predictive values in percentages. The classifier achieved true positive rates over 90% for more than half of the classes, only the OpenCI class being below 80% with a value of 78.6%. Positive predictive values were also over 90% for most classes, with only ClosedOI compounds being below 80%. Overall, the classifier correctly sorted the compounds into the 13 classes in 92.05% of cases. However, the classifier was not able to sort the stuck versions of those compounds whose differences in the unbinding rates between the preferential and non-preferential binding states were close to two orders of magnitude. In these cases, the classifier predicted the preferential binding state, but it failed to guess whether it binds to any other state. We ran voltage clamp and unicellular simulations to check if the effects of these different drugs were similar, provided they have the same preferential state. We verified that their transitory and the stationary effects depended on the value of the dissociation rate for the preferential binding state and not on the number of simultaneously blocked states. Fig. 6 shows some exam-

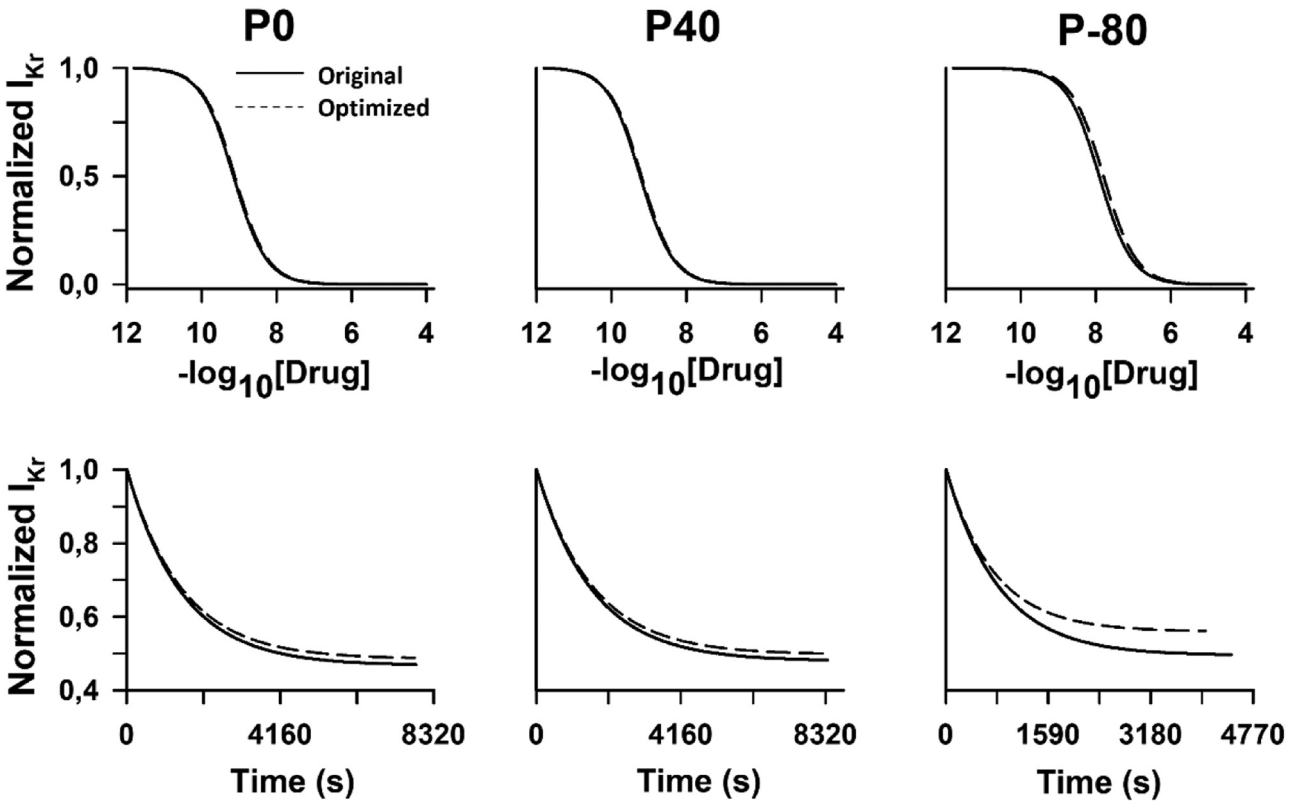

Fig. 3. Hill plots (top) and onset of I_{Kr} block, normalized tail current amplitudes for each sweep of the voltage clamp, (bottom) at the respective IC_{50} for the dofetilide model (InactiveO) for the P0 (left column), P40 (middle column) and P-80 (right column).

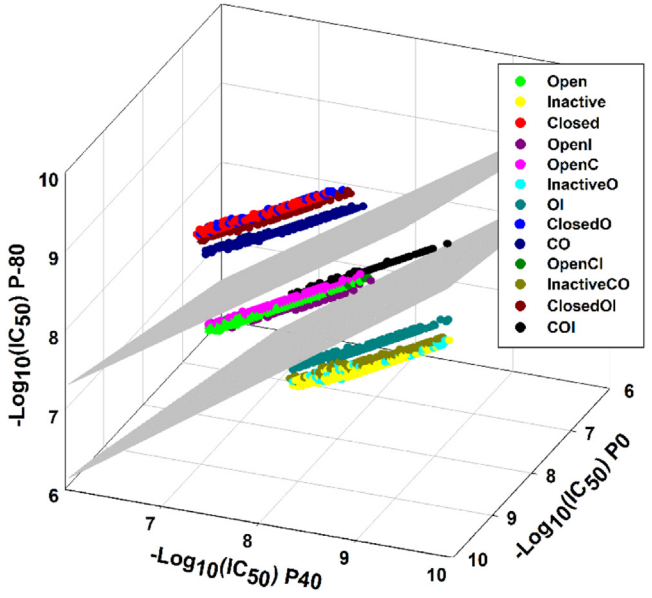

Fig. 4. 3D representation of the IC_{50} values of all the training stuck 100R virtual drugs and the decision surfaces separating the three groups of compounds with closed (top), open (middle) or inactivated (bottom) state preference.

ples of the onset of I_{Kr} block for stuck 100R open state-preference compounds, comparing the behaviors of Open, OpenC, OpenI and OpenCI drugs with the same diffusion rate and the same dissociation rate for the preferential binding state using the three voltage clamp protocols at their respective IC_{50} concentrations. The four possibilities exhibit similar onset of I_{Kr} block with the three voltage clamp protocols. Moreover, the time courses of the steady state action potential and of the I_{Kr} during IC_{50} drug exposure are alike (insets). Therefore, the drugs whose differences in the unbinding rates between the preferential and non-preferential binding states were close to two orders of magnitude could be mathematically modeled fairly accurately assuming any of the classes that have the same preferential state. Even though this phenomenon is characteristic of the stuck drugs with two orders of magnitude of difference between the dissociation rates of the preferential and non-preferential binding states, we evaluated the performance of the classifier on predicting the state preference for drug binding. To do so, Open, OpenC, OpenI and OpenCI drugs were grouped into one subclass called open preference. Inactive, InactiveO and InactiveOI were grouped into another one called inactive preference. Closed, ClosedO and ClosedOI were grouped into another one called closed preference and lastly, the remaining drugs were grouped into another one called no preference. The lower table of Fig. 5 shows the confusion matrix for this classification where all groups have over 90% accuracy.

4.1. Fitting of the diffusion and dissociation rates

To elucidate the diffusion and dissociation rates of a given compound, an optimization tool based on the iterative Nelder-Mead simplex algorithm [30] was used, as in previous works [31–33]. Rates values of the drug models were optimized considering the class assigned by the classifier and the parameters for each protocol.

The core of the optimization tool evaluates a pair of diffusion and dissociation rates by simulating the protocols at the corresponding IC_{50} concentration of the target drug. The error obtained with these rates is calculated as the addition of 6 components. They are computed as the absolute values of the differences in the time constants and the percentages of block produced by the sim-

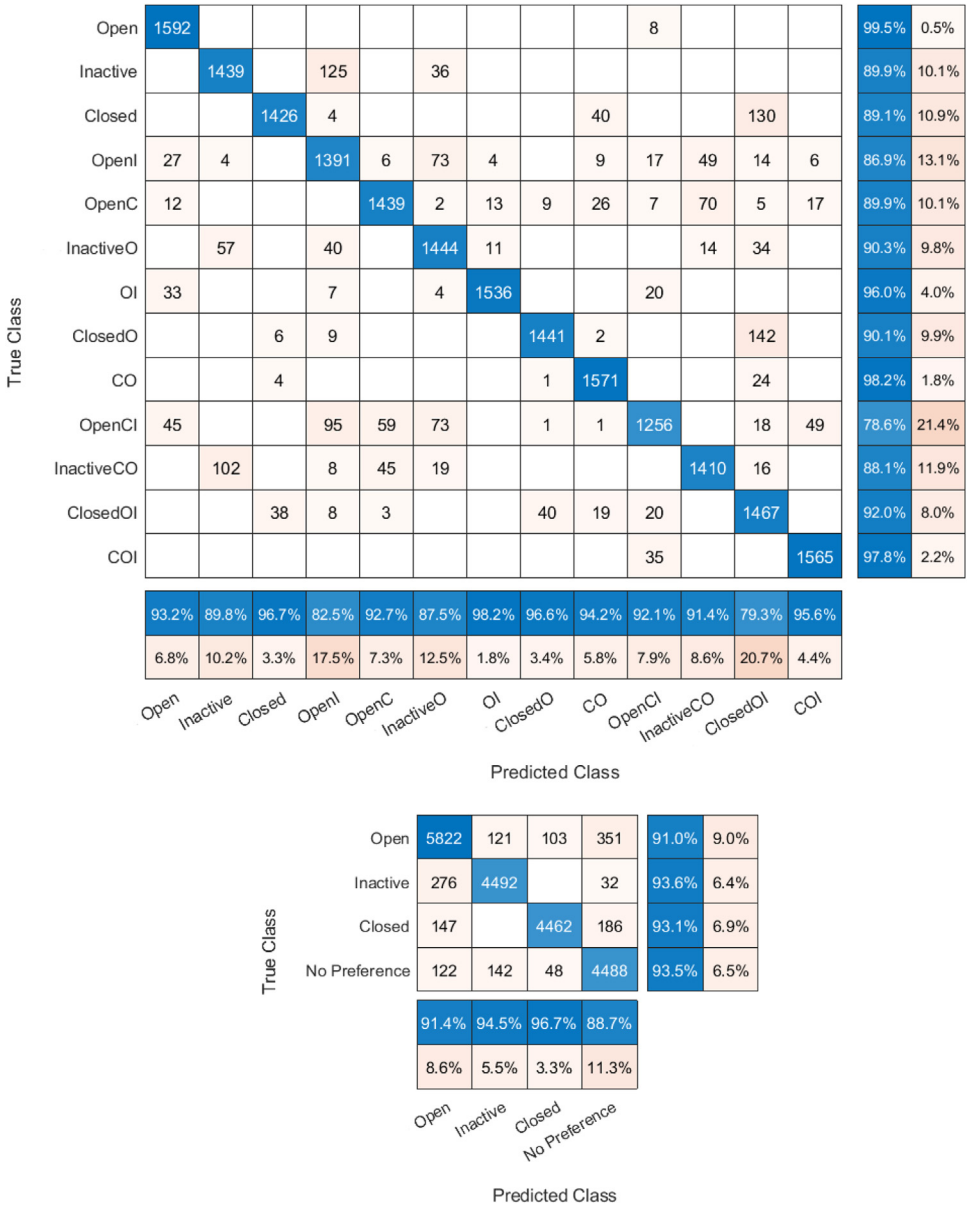

Fig. 5. Confusion matrices of the classifier when considering all the 13 classes of drugs (top table) and when only considering the state preference for drug binding (bottom table). Correctly classified drugs are represented in blue. Numbers in each box indicate the number of drugs. Rightmost columns show the true positive rate in percentage and bottommost rows show the positive predictive value in percentage.

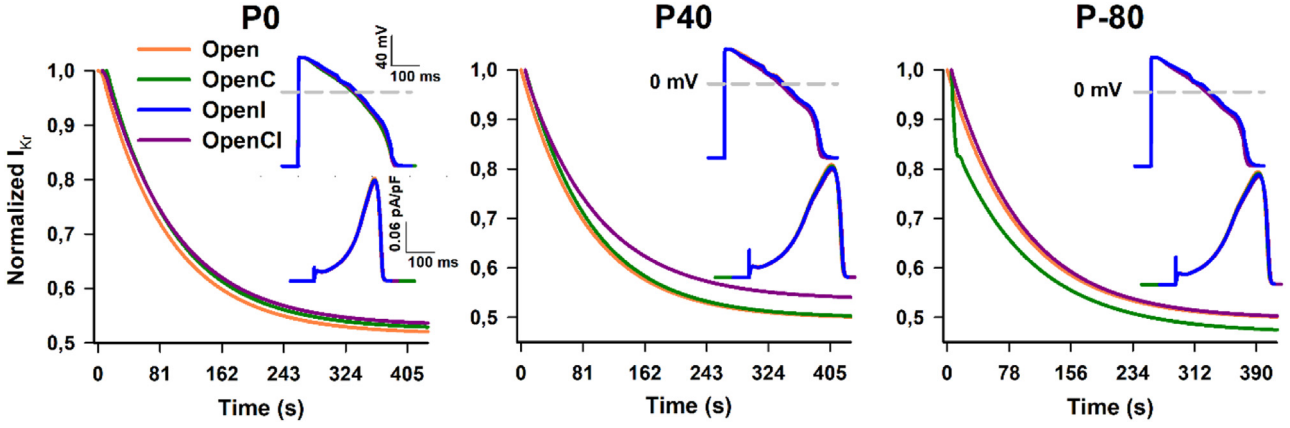

Fig. 6. Onset of I_{Kr} block. Normalized tail current amplitudes for each sweep of the voltage clamp protocol are plotted as a function of time under exposure to the IC_{50} for drugs with high open state preference using P0 (left), P40 (middle) and P-80 (right). Insets illustrate the steady state action potentials at 1 Hz (top) and I_{kr} at 1 Hz (bottom) at their respective IC_{50}. The diffusion rate for the preferential binding state (Open) is 9.68 $\mu M^{-1}s^{-1}$ and the dissociation rate is 0.0012 s^{-1}.

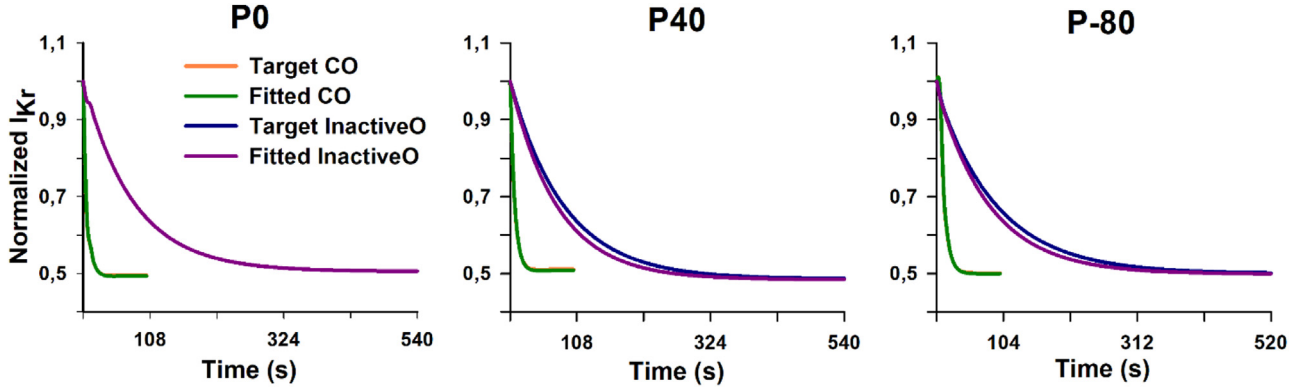

Fig. 7. Comparison of the fitted and target onset of I_{Kr} block. Time courses of the normalized tail current amplitudes for each sweep of the voltage clamp protocol under exposure to the IC_{50} of CO and InactiveO drugs using P0 (left), P40 (middle) and P-80 (right) are plotted as a function of time.

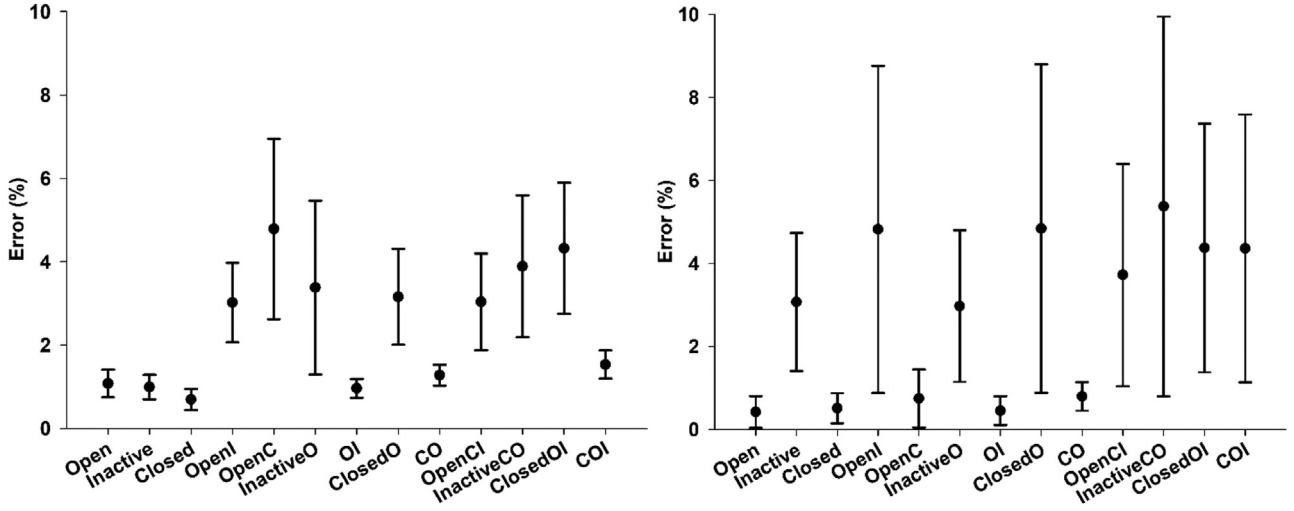

Fig. 8. Errors in the current inhibition at the IC_{50} concentrations (left) and in the fitted transition rates (right). Black dots represent the mean error per class and the lines are the 95% confidence interval boundaries.

ulated drug and the target for each protocol. Fig. 7 depicts the onset of I_{Kr} block obtained from the optimization of a CO and InactiveO compound. This figure shows that the optimized compounds closely resemble the target ones.

The errors between the results obtained by the automatically generated models and those produced by the original compounds were computed in order to quantify the accuracy of the fitting process. Fig. 8 shows the calculated mean errors in the current inhibition at the IC_{50} concentrations and in the fitted rates for the 13 classes along with the 95% confidence interval. The mean errors for each class are below 5% and the 95% confidence intervals are below 8% and 10%, respectively. The total mean values of the errors are 2.47% and 2.77%, respectively. For the specific case of dofetilide, the errors are 6.76% and 1.97%, respectively. Therefore, our system could be very useful to simulate the dynamic drug–hERG channel interactions.

4.2. Considerations about the experimental variability of the IC_{50}

As experimental characterization of IC_{50} is affected by the experimental variability, we wanted to assess the performance of our classifier in the presence of this variability. For this purpose, 16 compounds for each of the 13 classes were selected and 10 random variations were generated for each compound, making a total of 2080 drugs. For this new set of drugs, the IC_{50} values were taken from normal distributions with the original IC_{50} values and a standard deviation of 20%. The confusion matrix for this new set of drugs is shown in Fig. 9. The classifier achieved true positive rates and positive predictive values over 80% and 75%, respectively, for more than half of the classes. The total accuracy in predicting the class was 78.13%, which is slightly smaller than the one obtained without accounting for the experimental variability (92.05%), but it is a high value considering that the drugs are sorted into 13 classes. Therefore, our theoretical system shows a good performance when introducing levels of experimental variability encountered in real world experiments.

5. Discussion

In this work, we design a pipeline based on computer simulations that automatically generates Markovian dynamic drug models using data obtained from simple voltage clamp protocols, which would allow the simulation of more accurate clinical trials. Our system automatically tailors the structure of the Markovian model and fits the necessary parameters to capture the states where the drug binds and unbinds, the preferential state-dependent binding properties, the relative affinities, trapping and non-trapping dynamics and the onset of I_{Kr} block. Moreover, the computational requirements are low and the generation of the model of the drug-hERG channel interaction from the voltage clamp data can be performed quite quickly on a common desktop computer. For this purpose, we used three specific voltage clamp protocols, P0, P40 and

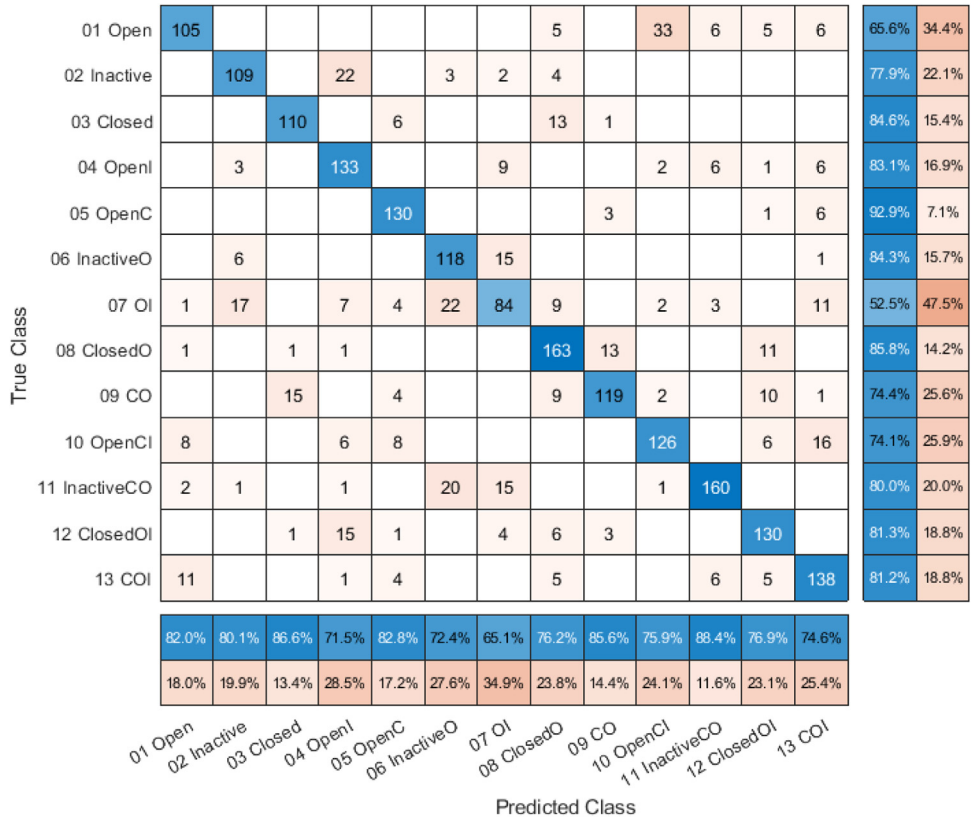

Fig. 9. Confusion matrix of the classifier when considering experimental variability on the IC_{50}. Correctly classified drugs are represented in blue. Numbers in each box indicate the number of drugs. Rightmost columns show the true positive rate in percentage and bottommost rows show the positive predictive value in percentage.

P-80, which maximize the time the channel occupies the open, inactivated and closes states, respectively. For each protocol-drug pair we calculate the IC_{50} value and the time constant of the onset of I_{Kr} block, which are highly dependent on drug dynamics and kinetics. We have developed a classifier based on machine learning techniques and optimization algorithms to create the drug models, whose accuracies are 92% and 97.38%, respectively. This pipeline has been theoretically tested with dofetilide and has obtained an accuracy of 95.64%, which supports the potential utility for a clinical research of our pipeline.

5.1. Development of the model

Tools for fitting dynamic models for different I_{Kr} blockers have previously been developed using data from voltage clamp protocols by Li et al. [13]. These authors used a unique Markov model chain and fitted certain parameters of the model. That approach has represented a step further in the assessment of proarrhythmic risk. However, some unexpected behaviors have been reported. Indeed, some of the proposed drug models fail to achieve total block of the current even at high concentrations [34], such as cisapride, which does not reach even the 50% block at high concentrations when stimulated with some of our voltage clamp protocols. Moreover, such implementation is computationally highly demanding. The group of Clancy [35,36] have also developed a computational pipeline to generate dynamic models of I_{Kr} blockers, such as dofetilide, moxifloxacine and sotalol, with the aim of predicting cardiac cardiotoxicity. Their models are based on data from physics-based computer models that account for channel conformational state and drug ionization state specific atomic-scale determinants of drug-hERG channel interaction as well as molecular dynamics simulations, instead of voltage clamp protocols. They use the Markov chain proposed by Fink and coworkers [15], as in our work, and consider drug binding and unbinding to the open and to the inactivated states allowing the change of the conformational state in drug-bound channels, as in our unstuck versions of Open and InactiveO drugs. Their models differentiate neutral, cationic, and zwitterionic states of the drugs, unlike ours. Pearlstein and colleagues [37] used modeling and simulation to characterize the effects of channel gating and binding kinetics on hERG occupancy and on its inhibition on the human ventricular action potential. They modeled hERG blockers dynamics allowing drug bound channels to change their conformational state and considering binding and unbinding to the open and inactivated states, and unbinding to the close state, but not binding to the closed state, just trapping. They found that the evolution of the occupancies during the action potential differed between trapping and non-trapping drugs.

Our drug-channel interaction model is based on the Fink et al. 2008 [15] I_{Kr} formulation. In our previous work [12], we compared dug-channel interactions using Fink et al. 2008 [15], Lee et al. 2019 [11] and Li et al. 2017 [13] markovian models. In that study, we simulated the Hill plots for each type of the prototypical drugs binding to two states with state-dependent affinities using the proposed protocols. We observed that the tendencies of the patterns of the Hill plots obtained with the three approaches were very similar. Therefore, it suggests a low dependence of our pipeline with the I_{Kr} model, although quantitative differences could be found if the abovementioned hERG formulations were used.

In this study, we propose a novel approach based on voltage clamp protocols, where a wider range of possibilities is considered. For example, drugs may bind to any state (individually or simultaneously) and the conformational states changes are restricted or allowed when the drug is bound. 12 Markovian chains are needed

in our approach (see Fig. 1) in order to account for these aspects. In this work, we propose a new methodology for the development of models considering kinetics and dynamics drug-hERG channel interaction using the outputs provided by our classifier and an optimization tool. The results obtained by our system accurately resemble the characteristics of the studied virtual drugs. The whole process usually takes less than an hour in an Intel Core® i7-4790 3.60 GHz CPU with 16 Gb of RAM memory.

5.2. Voltage clamp protocol dependency

The IC_{50} has been reported to have a high degree of variability depending on the voltage clamp protocol used to determine it [7-9,11]. Lee and colleagues published a very interesting work showing that state preference drug binding can be quantified using protocol-dependent differences in IC_{50} values [11], which has been shown to play an important role in action potential prolongation [27,38]. Lee and coworkers used a simple Markov model that considered drug binding in the open and inactivated states that did not allow drug-bound channels to change its conformational state without drug unbinding, nor trapping, but that was good enough to reveal highly relevant insights. In our work, we use a more complete Markov description of drug binding, which captures the preferential state-dependent binding properties, the relative affinities, trapping and non-trapping dynamics and the onset of I_{Kr} block, that would further improve predictions based on voltage clamp data. It is also worth mentioning that, as the variety of drug dynamics used in our study is very wide, characterization of drug-channel interaction was a challenge. Following the evidence that state preference drug binding can be quantified using protocol-dependent differences in IC_{50} values, we have used three previously developed voltage clamp protocols [12]. These protocols were specifically designed to maximize the probability of the potassium hERG/I_{Kr} channels to occupy the closed, open or inactivated states. Our results show that the IC_{50} is dependent on the kinetics and dynamics of the drug. For example, stuck drugs which preferentially bind to the inactive state will have higher IC_{50} values when measured with protocol P-80 (which maximizes the closed state channel occupancy) than with P0 or P40. This is shown in Fig. 4, where the inactive state preference group is distributed under the other two groups. Our approach takes into account these differences to accurately elucidate the binding states and the preferential one.

5.3. Prediction of the preferential blocking states

Recent studies have shown the benefits of combining machine learning techniques and in silico simulations to extract features from data sets [39,40]. Our work supports the fact that the variability in the IC_{50} occurs in a predictable way when considering the binding states and the relative affinities [11], as seen in the linear behaviors observed in Fig. 4. Therefore, we decided to use supervised machine learning techniques to classify the drugs.

In our study, we limited the number of voltage clamp protocols to three well designed ones, maximizing the potential differences. Our protocols are crucial for the good performance shown by the classifier in both aspects, the accurate prediction of the compound behavior and the time required, taking only a few seconds for the process to be completed.

5.4. Limitations

Firstly, while we have considered a wide range of virtual compounds regarding blocked states and the speed of the blocking, the lack of experimental data to validate our system is the main limitation of our study. Secondly, the temperature was set at 22 °C because the vast majority of voltage clamp experiments for cardiac safety assessment of pharmacological compounds at the early stages of drug development are performed at room temperature. Our methodology could be adapted to be used with data obtained at a physiological temperature as the Fink et al. model includes the dependence of the ionic current with the temperature, so it could be done in a following step. Lastly, it would also be interesting for a future work to assess whether drug binding states affect gating kinetics. For example, knowing if an inactive affinity compound has slower inactivation.

All in all, we believe that these limitations do not jeopardize the main conclusions and that our study proposes a promising tool to elucidate the states of binding and binding state-preference and the ratios of the unbinding rates of a given compound and to estimate the transition rates to generate an accurate dynamic model.

6. Conclusion

In this work, we propose a new methodology that not only classifies drugs depending on the affinities to the channel states but also generates dynamic drug models automatically, accurately and quickly, which covers an urgent need in the field and will contribute to the deployment of in silico models in the pharmaceutical industry. These models reproduce the preferential state-dependent binding properties, the relative affinities, trapping and non-trapping dynamics and the onset of the I_{Kr} block, which paves the way for the performance of in silico clinical trials reproducing dynamic drug-hERG channel interactions using data from simple voltage clamp protocols.

Patenting of the proposed system and/or software is under consideration.

Ackowledgments

This work was the Spanish Ministerio de Ciencia, Innovación y Universidades [grant “Formación de Profesorado Universitario” FPU19/02200; grant PID2019-104356RB-C41 funded by MCIN/AEI/10.13039/501100011033]; the European Union’s Horizon 2020 research and innovation program [grant agreement No 101016496 (SimCardioTest)]; and the Dirección General de Política Científica de la Generalitat Valenciana [grant PROMETEO/2020/043]. Patenting of the proposed system/software is under consideration.

References

[1] Gintant, et al., Preclinical torsades-de-pointes screens: advantages and limitations of surrogate and direct approaches in evaluating proarrhythmic risk, Pharmacol. Ther. 119 (2008) 199–209.
[2] Food and Drug Administration, International conference on harmonisation; guidance on S7B nonclinical evaluation of the potential for delayed ventricular repolarization (QT Interval Prolongation) by human pharmaceuticals, Fed. Regist. 70 (2005) 61133–61134.
[3] Sager, et al., Rechanneling the cardiac proarrhythmia safety paradigm: a meeting report from the cardiac safety research consortium, Am. Heart J. 167 (2014) 292–300.
[4] Witchel, et al., Troubleshooting problems with in vitro screening of drugs for QT interval prolongation using HERG K+ channels expressed in mammalian cell lines and xenopus oocytes, J. Pharmacol. Toxicol. Methods 48 (2002) 65–80.
[5] Stork, et al., State dependent dissociation of HERG channel inhibitors, Br. J. Pharmacol. 151 (2009) 1368–1376.
[6] Hancox, et al., The HERG potassium channel and HERG screening for drug-induced torsades de pointes, Pharmacol. Ther. 119 (2008) 118–132.
[7] Kirsch, et al., Variability in the measurement of HERG potassium channel inhibition: effects of temperature and stimulus pattern, J. Pharmacol. Toxicol. Methods 50 (2004) 93–101.
[8] Yao, et al., Estimation of Potency of HERG Channel Blockers: Impact of Voltage Protocol and Temperature, J. Pharmacol. Toxicol. Methods 52 (2005) 146–153.
[9] Milnes, et al., Investigating dynamic protocol-dependence of hERG potassium channel inhibition at 37°C: Cisapride versus dofetilide, J. Pharmacol. Toxicol. Methods 61 (2010) 178–191.

[10] Windley, et al., The temperature dependence of kinetics associated with drug block of hERG channels is compound-specific and an important factor for proarrhythmic risk prediction, Mol. Pharmacol. 94 (2018) 760–769.
[11] Lee, et al., Protocol-dependent differences in IC50 values measured in human ether-á-go-go-related gene assays occur in a predictable way and can be used to quantify state preference of drug binding, Mol. Pharmacol. 95 (2019) 537–550.
[12] Gomis-Tena, et al., When Does the IC50 Accurately Assess the Blocking Potency of a Drug? J. Chem. Inf. Model. 60 (2020) 1779–1790.
[13] Li, et al., General principles for the validations of proarrhythmia risk prediction models: an extension of the CiPA in silico strategy, Pharmacol. Ther. 107 (1) (2020) 102–111.
[14] International council for harmonisation of technical requirements for pharmaceuticals for human useGeneral Considerations for Clinical Studies E8(R1), 2021.
[15] Fink, et al., Contributions of HERG K+ current to repolarization of the human ventricular action potential, Prog. Biophys. Mol. Biol. 96 (2008) 357–376.
[16] Wang, et al., Modulation of HERG affinity for E-4031 by [K+]o and C-type inactivation, FEBS Lett 417 (1997) 43–47.
[17] Ficker, et al., Molecular determinants of inactivation and dofetilide block in ether a-go-go (eag) channels and eag-related K+ channels, Mol. Pharmacol. 60 (2001) 1343–1348.
[18] Kamiya, et al., Molecular determinants of hERG channel block by terfenadine and cisapride, J. Pharmacol. Sci. 108 (2008) 301–307.
[19] Yao, et al., Estimation of potency of HERG channel blockers: impact of voltage protocol and temperature, J. Pharmacol. Toxicol. Methods 52 (2005) 146–153.
[20] Dumaine, et al., Blockade of HERG and Kv1.5 by ketoconazole, J. Pharmacol Exp Ther. 286 (1998) 727–735.
[21] Milnes, et al., Preferential closed channel blockade of HERG potassium currents by chemically synthesised BeKm-1 scorpion toxin, FEBS Lett 547 (2003) 20–26.
[22] Alexandrou, et al., Mechanism of hERG K+ channel blockade by the fluoroquinolone antibiotic moxifloxacin, Br. J. Pharmacol. 147 (2006) 905–916.
[23] Kamiya, et al., Molecular Determinants of hERG Channel Block, Mol. Pharmacol. Sci. 69 (2006) 1709–1716.
[24] Stork, et al., State dependent dissociation of HERG channel inhibitors, Br. J. Pharmacol. 151 (2007) 1368–1376.
[25] Windley, et al., Measuring kinetics and potency of hERG block for CiPA, J Pharmacol. Toxicol. Methods 87 (2017) 99–107.
[26] Perrin, et al., Drug binding to the inactivated state is necessary but not sufficient for high-affinity binding to human ether-à-go-go-related gene channels, Mol. Pharmacol. 74 (2008) 1443–1452.
[27] Romero, et al., In silico screening of the impact of hERG channel kinetic abnormalities on channel block and susceptibility to acquired long QT syndrome, J. Mol. Cell. Cardiol. 87 (2015) 271–282.
[28] Hill, et al., Kinetics of drug interaction with the Kv11,1 potassium channel, Mol Pharmacol 85 (2014) 769–776.
[29] O'Hara, et al., Undiseased human cardiac ventricular action potential: model formulation and experimental validation, PLoS Comput. Biol. 7 (2011) e1002061.
[30] Nelder, R. Mead, A simplex method for function minimization, The Comp. J. 7 (4) (1965) 308–313.
[31] Moreno, et al., Ranolazine for congenital and acquired late I Na-linked arrhythmias, Circulation Research 113 (7) (2013) 50–61.
[32] Moreno, et al., Parameterization for in-silico modeling of ion channel interactions with drugs, PLoS ONE 11 (3) (2016) e0150761.
[33] Escobar, Modelado y Simulación de Mutaciones Causantes de la Taquicardia Ventricular Polimórfica Catecolaminérgica, Dept. Electron. Eng. Polytechnic University of Valencia, Valencia, Spain, 2019 M.S. thesis.
[34] Wang, et al., Towards an understanding of hERG potency variability derived from patch clamp protocols, J. Pharmacol. Toxicol. Methods 105 (107) (2020) 41.
[35] Yang, et al., A computational pipeline to predict cardiotoxicity: from the atom to the rhythm, Circ. Res. 126 (2020) 947–964.
[36] DeMarco, et al., Molecular determinants of pro-arrythmia proclivity of d- and l-sotalol via a multi-scale modeling pipeline, J. Mol. Cell Cardiol. 158 (2021) 163–177.
[37] Pearlstein, et al., Implications of dynamic occupancy, binding kinetics, and channel gating kinetics for hERG blocker safety assessment and mitigation, Curr. Top. Med. Chem. 16 (2016) 1792–1818.
[38] Lee, et al., In silico assessment of kinetics and state dependent binding properties of drugs causing acquired LQTS, Prog. Biophys. Mol. Biol. 120 (2016) 89–99.
[39] Feeny, et al., Artificial intelligence and machine learning in arrhythmias and cardiac electrophysiology, Circ. Arrhythm. Electrophysiol. 13 (2020) e007952.
[40] Vamathevan, et al., Applications of machine learning in drug discovery and development, Nat. Rev. Drug Discov. 18 (2019) 463–477.